





Open Archive Toulouse Archive Ouverte (OATAO)

OATAO is an open access repository that collects the work of Toulouse researchers and makes it freely available over the web where possible

This is an author's version published in: <http://oatao.univ-toulouse.fr/24473>

Official URL: <https://doi.org/10.1166/jcsb.2016.1150>

To cite this version:

Lakbita, Omar  and Rhouta, Benaïssa and Maury, Francis and Senocq, François 
and Amjoud, M'barek and Jada, Amane *Supported Photocatalyst Based on CuO–TiO₂/Palygorskite Nanocomposite Material for Wastewater Treatment*. (2016)
Journal of Colloid Science and Biotechnology, 5 (2). 199-205. ISSN 2164-9634

Any correspondence concerning this service should be sent
to the repository administrator: tech-oatao@listes-diff.inp-toulouse.fr

Supported Photocatalyst Based on CuO–TiO₂/Palygorskite Nanocomposite Material for Wastewater Treatment

O. Lakbita^{1,2}, B. Rhouta^{1,*}, F. Maury², F. Senocq², M. Amjoud¹, and A. Jada³

¹Laboratoire de Matière Condensée et Nanostructures (LMCN), Faculté des Sciences et Techniques Guéliz, Université Cadi Ayyad, BP 549, Marrakech, Maroc

²Cirimat, Université de Toulouse, CNRS-UPS-INP, ENSIACET, 4 allée Emile Monso, BP, 44362, 31030 Toulouse, Cedex 4, France

³Institut de Sciences des Matériaux de Mulhouse (IS2M), CNRS UMR 7361, 15 rue Jean Starcky, BP 2488, 68057 Mulhouse Cedex, France

This study deals with the immobilization of mixtures of two semiconductor oxides CuO and TiO₂ on fibrous palygorskite clay mineral in order to evaluate their photocatalytic activity for removing Orange G dye as model pollutant from aqueous solutions. The elaboration of CuO–TiO₂/Palygorskite nanocomposites was carried out by impregnation with Cu²⁺ of before hand synthesized TiO₂ supported palygorskite (Pal) followed by air annealing for 5 h at 550 °C. In the composite materials, different CuO to CuO + TiO₂ molar ratios were used in order to obtain a CuO content in the range 13–30 mol.%. XRD, SEM and TEM equipped with elemental EDS analysis are concordant for showing the crystallization of anatase TiO₂ along with CuO whose average size of nanoparticles (NPs) are in the range 6 to 20 nm as determined by TEM. By increasing the CuO content the average size of this oxide remains constant at about 10 nm while that of TiO₂ NPs is slightly decreasing from 8.4 to 5.1 nm. Both oxide NPs were successfully attached on palygorskite fibers where they form CuO–TiO₂ heterojunctions (grain boundaries like). The CuO–TiO₂/Pal supported photocatalyst containing 23% of CuO was found to be the most photoactive material but it remained less active than TiO₂/Palygorskite supported photocatalyst. The photocatalytic activity of the mixed nanocomposites is not readily correlated with only one of their main features as CuO content or the average crystallite size of functional oxides indicating that if there are synergistic effects there are also antagonistic effects in particular for high CuO contents.

Keywords: Palygorskite, TiO₂, CuO, Semiconductor, Heterojunction, Photocatalysis, Wastewater Treatment.

1. INTRODUCTION

During the last decades, heterogeneous photocatalytic oxidation has raised a huge interest in the field of industrial wastewater treatment.^{1–4} Its principle is based on the formation of strong oxidant species, namely photoholes (h⁺) and/or hydroxyl radicals (·OH) upon the irradiation of a semiconductor (SC) oxide (e.g., TiO₂, ZnO, Fe₂O₃, WO₃, ZrO₂, SrO₂, CeO₂...) with a photon source (hν) higher than the band gap energy of SC oxide.⁵ The generated reactive entities are able to produce a complete mineralization of organic pollutants into CO₂ and H₂O.³ In this respect, TiO₂ in the form of anatase was found to be one of the most photoactive SC oxide and hence the most used owing to its low cost, safety and chemical inertia.³

Nevertheless, the use of TiO₂ in the form of powder, especially in commercially available products as Degussa P25, arises drawbacks due to firstly the easy agglomeration of fine particles inducing the reduction of photonic efficiency for most degradation processes to less than 10% and, on the other hand, the requirement for being recovered from water decontaminated by TiO₂ slurry to implement costly microfiltration processes.³

For overcoming these issues, several works were recently devoted to the immobilization of TiO₂ on porous supports endowed of large surface area such as glass fibers,⁶ silicon gels,⁷ zeolites,⁸ activated carbons^{3,9} and clay minerals.^{10–14} In this context, Bouna et al.^{15,16} and Rhouta et al.¹⁷ showed the beneficial effect of the use of clay minerals such as stevensite, palygorskite and beidellite as porous supports on the achievement of on one

*Author to whom correspondence should be addressed.

hand, the monodisperse distribution of TiO₂ nanoparticles and, on the other hand, the remarkable stabilization of most photoactive metastable anatase phase allowing the huge improvement of photocatalytic degradation of dyes.

Nevertheless, the photocatalytic activity of TiO₂ could be further improved by doping the SC oxide with heteroatoms (C, N, S),^{18–24} transition metals (V, Cr, Fe, Co, Ni)²⁵ and recently by the formation of heterojunctions between anatase TiO₂ and a semiconductor oxide endowed with smaller band gap energy such as CdS, WO₃, Fe₂O₃ and CuO which plays the role of sensitizer.²⁶ Thus CuO is a *p*-type semiconductor with a direct band gap energy of 1.2 eV while TiO₂ anatase is an *n*-type semiconductor with a larger band gap energy of 3.2 eV. A mixture of such semiconductor oxides exhibits a good photocatalytic activity thanks to *p*–*n* heterojunctions that limit recombination of charge carriers.²⁷ For instance, Behnadjady et al.²⁸ reported the elaboration of CuO/TiO₂ composites by chemical impregnation method of TiO₂. Degussa P25 nanoparticles with Cu²⁺ ions. The impregnation of TiO₂ Degussa P25 by 0.05 mol% of Cu²⁺ yielded upon calcinations at 450 °C for 3 h to a material more photoactive than pristine TiO₂ Degussa P25. In the same way, Fang et al.²⁹ achieved by means of hydrothermal method the functionalization of graphene oxide with NPs of CuO/TiO₂ composite within the Cu:Ti molar ratio of 0.33. The developed supported photocatalyst was found to be four times more active than Degussa P25, by removing after 8 h almost 80% of methylene blue under as well as UV than visible light irradiations.

The present study reports the preparation in two steps of CuO–TiO₂ supported palygorskite composites. TiO₂ supported palygorskite was first developed by sol–gel according to the method reported by Bouna et al.¹⁵ which was thereafter impregnated with Cu²⁺ and afterwards air heat-treated at 550 °C for 5 h. The developed CuO–TiO₂ supported palygorskite was characterized by XRD, SEM and TEM equipped with EDS analysis. Afterwards, the catalytic activity of developed clay supported photocatalyst was assessed towards the removal of Orange G (OG) dye from aqueous solutions.^{11, 12, 30, 31} This anionic dye compound was selected as model pollutant because its adsorption onto clay minerals was negligible due to electrostatic repulsion between the negatively charged clay particles and the dye molecules.³²

2. EXPERIMENTAL DETAILS

2.1. Materials

Titanium tetra-isopropoxide (TTIP) of 99.999% purity, isopropanol, hexadecyltrimethyl ammonium bromide (CTAB), trihydrated copper nitrate (Cu(NO₃)₂ · 3H₂O) and anionic dye orange G (OG) chemicals were purchased from Aldrich and used without further purification. Natural raw clay was sampled from Marrakech High-Atlas region.

It was reported to be made up of about 30% of carbonates in the forms of calcite and ankerite, 5% of quartz and 65% of fine clay fraction (<2 μm). Upon purification and Na⁺ saturation, the isolated <2 μm Na⁺-homoionic fraction was found to be exclusively fibrous since it is predominated by around 95% of palygorskite along with almost 5% of sepiolite so that it was labeled Pal.²⁵ It was first purified and homoionized with Na⁺ ions according to the procedure described in details elsewhere.³³ The derivative Na⁺-exchanged palygorskite (designed Na⁺-Pal) was thoroughly characterized to have cationic exchange capacity (CEC), BET surface area and total porous volume of 21.2 meq.100 g⁻¹, 116 m²g⁻¹ and 0.458 cm³ g⁻¹ respectively.³³

The composition of this palygorskite was found on the basis of 26 oxygen atoms to be (Si_{7.97}Al_{0.03}) (Mg_{2.17}Al_{1.46}Fe_{0.40}Ti_{0.05}) (Ca_{0.03}Na_{0.07}K_{0.03}) O_{20.18}(OH)_{1.94}(H₂O)_{3.88} · 2.43H₂O.³³

2.2. CuO–TiO₂/Palygorskite Composites Preparation

As beforehand mentioned, the preparation of CuO–TiO₂ supported palygorskite was achieved into two steps involving first the synthesis of TiO₂/Palygorskite composite which is afterwards impregnated with Cu²⁺ ions according to an adapted chemical method described elsewhere.³⁴

TiO₂ supported palygorskite composite material (labeled TiO₂/Pal) was prepared starting from Na⁺-exchanged purified palygorskite (Na⁺-Pal) according to the colloidal sol–gel procedure in two steps described in details elsewhere.¹⁵ Briefly, the synthesis route first involved the preparation of organo-palygorskite (CTA⁺-Pal) by ion exchange of Na⁺-Pal aqueous dispersion (1 wt.%) with 0.2 g of CTAB. Afterwards, 5 cm³ of TTIP in isopropanol were added to 1 g of CTA⁺-Pal dispersed in 7 cm³ of isopropanol and it was hydrolyzed and condensed by adding some water droplets to give rise to the gel precursor CTA⁺-Pal-Ti. Thereafter, the annealing in air at 600 °C for 1 h converted CTA⁺-Pal-Ti into TiO₂/Palygorskite nanocomposite (designated TiO₂-Pal). Assuming that 100% of TTIP is converted in to titania the concentration of TiO₂ into the composite TiO₂/Pal is 16.9 mmol for 1 g of palygorskite.

For preparing CuO–TiO₂/Pal nanocomposites, 1 g of TiO₂/Pal composite was first dispersed under stirring in 40 mL of an aqueous solutions of different masses of Cu(NO₃)₂ · 3H₂O (0.25, 0.5 and 0.75 g) in the ambient atmosphere during 48 h in order to allow Cu²⁺ ions to penetrate inside the bulk of the TiO₂/Pal material. Afterwards, supernatant was evaporated during 12 h at 80 °C in an oven. The obtained compounds precursors were thereafter heat-treated in air at 550 °C for 5 h to obtain mixed CuO–TiO₂/Pal composite materials with three different CuO content defined by the mole ratio CuO/(CuO + TiO₂) as 13, 23 and 30 mol.% and labeled 13% CuO–TiO₂/Pal, 23% CuO–TiO₂/Pal and 30% CuO–TiO₂/Pal, respectively.

2.3. Characterization Techniques

Structural properties of different elaborated TiO₂ and CuO–TiO₂ supported palygorskite nanocomposites were characterized by X ray diffraction (XRD) at room temperature in the same 2θ angular range [3°–60°] by using a Bruker D8 diffractometer equipped with a LynxEye detector (Bragg–Brentano configuration; Ni filtered Cu Kα radiation).

A Jeol JSM 6400 scanning electron microscope (SEM) equipped with an Oxford energy dispersive spectrometer, EDS (Si–Li detector; MK program) and a JEOL JEM 2100F transmission electron microscopy (TEM) equipped with a Bruker AXS Quantax EDS analyzer were used for characterizing clay particles and performing local elemental analysis.

2.4. Evaluation of Photocatalytic Activity

The photocatalytic activity of different samples was evaluated by measuring the decomposition rate of 25 mL of OG aqueous solutions (10^{−5} M) containing a dispersion of 25 mg of photocatalyst in a batch reactor under UV radiations by using an HPLN Philips 125 W lamp emitting at 365 nm. The degradation reaction was carried out in a quartz vessel (40 × 20 × 36 mm³) transparent to wavelengths >290 nm which was placed in a thermostated chamber (25 °C). The reactor was irradiated with a photon flux of 1 mW · cm^{−2} by adjusting the distance to the lamp to simulate the UV intensity of solar spectrum on the earth.³⁵

To determine the dye concentration, aliquots were taken from the mixture at regular time intervals and centrifuged at 12500 rpm for 5 min. The OG concentration in the supernatant was determined by measuring the absorbance at 480 nm using a UV–VIS–NIR spectrophotometer (Perking Elmer lambda 19).

3. RESULTS AND DISCUSSION

3.1. Phases Identification

For comparison purpose, Figure 1 depicts the superposition of XRD diagrams of starting Na⁺-exchanged palygorskite (Na⁺-Pal), pure CuO compound, TiO₂ supported palygorskite (TiO₂/Pal) and CuO–TiO₂ supported palygorskite composites differing in CuO content. In agreement with Bouna et al.¹⁵ and Rhouta et al.,³³ the XRD peaks observed in Na⁺-Pal at 8.36° (10.56 Å), 13.54° (6.51 Å), 16.30° (5.42 Å), 19.76° (4.47 Å), 20.80° (4.27 Å), 21.30° (4.20 Å) and 27.53° (3.23 Å) are characteristic of palygorskite clay mineral whose basal distance is about 10.56 Å. The peak at 26.6° (3.34 Å) is ascribed to remaining traces of accessory quartz SiO₂ (JCPDS file: 03-065-0466). It should be noted that among all these palygorskite peaks, only some harmonics at 19.76° (4.47 Å) and 27.53° (3.23 Å) are hardly observed in XRD patterns of both TiO₂/Pal composite and CuO–TiO₂ supported palygorskite mixed nanocomposites. For the sample

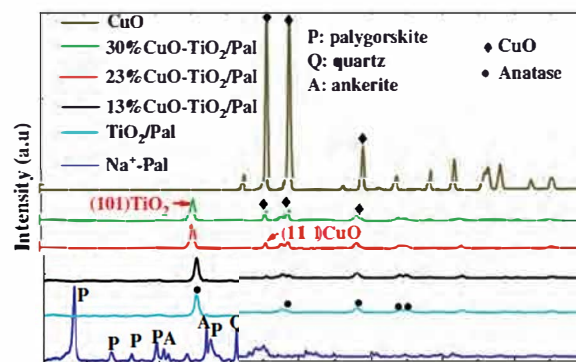


Fig. 1. Superposition XRD diagrams (from the bottom to the top) of Palygorskite (Na⁺-Pal), TiO₂/Pal composite, CuO–TiO₂/Pal mixed nanocomposites with increasing content of CuO (13%, 23% and 30%) and pure CuO.

TiO₂/Pal, reflections observed at 25.42° (3.50 Å), 37.95° (2.37 Å), 48.38° (1.88 Å), 53.96° (1.70 Å) and 55.22° (1.66 Å) correspond to anatase TiO₂ (JCPDS file 99-201-5379) denoting the occurrence of crystallization of only this crystalline phase in this nanocomposite in agreement with Bouna et al.¹⁵ All these reflections of TiO₂ anatase are also observed in the diffractograms of the three CuO–TiO₂/Pal composite materials in which besides appear additional peaks mainly at 35.50° (2.53 Å), 38.76° (2.32 Å) and 48.76° (1.86 Å). These additional peaks are also encountered in the XRD diagram of pure CuO powder which means that they are attributed to the CuO phase. These results denote the crystallization of CuO along with anatase TiO₂ in all synthesized CuO–TiO₂/Pal composite materials. The intensity of CuO reflections appears to increase with the increase of CuO amount in CuO–TiO₂/Pal composites. This is consistent with an increase of either the number or the size of CuO crystallites when the amount of copper precursor increased in the synthesis of the mixed nanocomposite.

The average crystallite sizes of TiO₂ anatase and CuO were determined from the full width at half maximum (FWHM) of the corresponding (101) TiO₂ and (111) CuO XRD peaks in CuO–TiO₂/Pal composites according to Scherrer's equation. The data are gathered in Table I. The average crystallite size of TiO₂ is slightly larger in TiO₂/Pal (8.4 nm) than in the mixed CuO–TiO₂/Pal nanocomposite materials (5.1–7.1 nm). Furthermore, in the CuO–TiO₂/Pal nanocomposite, it appears that anatase crystallite sizes sensibly decrease by increasing the CuO content above 23%. This gives evidence for steric effects and growth competition between the two oxides: the presence of CuO NPs likely hinder the growth of TiO₂ crystallites.

By contrast, the CuO crystallite sizes are constant in CuO–TiO₂/Pal composites regardless of the content of CuO. Consequently the increase of CuO XRD peaks is essentially due to an increase of the number of CuO NPs rather than an increase of their average crystallite size. This is important because the probability to form interfaces or

Table I. Photocatalytic data deduced from Figure 4. The oxide content in the 25 mg of composite used in photocatalytic test is also given as well as the average crystallite size of TiO₂ anatase and CuO assessed from the FWHM of the corresponding (101) and (111) XRD peaks, respectively. The CuO content in the composite correspond to the mole ratio CuO/(CuO+TiO₂).

Sample	Photocatalysis			Oxide content in photocatalytic test		Average crystallite size	
	Degradation rate at origin (min ⁻¹)	OG abatement after 120 min (%)	OG abatement after 240 min (%)	TiO ₂ mass (mg)	CuO mass (mg)	TiO ₂ (nm)	CuO (nm)
13CuO-TiO ₂ /Pal	0.003	28	40	13.2	1.9	6.9	10.1
23CuO-TiO ₂ /Pal	0.009	59	70	12.2	3.7	7.1	10.7
30CuO-TiO ₂ /Pal	0.007	44	52	11.4	5.1	5.0	10.1
TiO ₂ /Pal	0.010	90	100	14.2	–	8.4	–

grain boundaries is larger with small particles than with large ones. As a result, this significantly increases the probability to form heterojunctions between the two semiconductor materials.

3.2. Microstructural Characterizations

An overview of Na⁺-Pal morphology was afforded by SEM observations. Figure 2(a) shows fibers bundles confirming the fibrous character of the palygorskite clay mineral. As described elsewhere by Rhouta et al.,³³ the fibers appear either as well separated individual fibers or as bundles of several fibers having an average length of ca. 1 μm and a diameter ranging from 10 to 50 nm. These fibers are also observed in the mixed 30% CuO-TiO₂/Pal composite

(Fig. 2(b)) but with irregular shape and reduced length as a result likely of stirring and centrifugation underwent by the sample during preparation procedure. The palygorskite fibers appear embedded in nodular aggregates with an average size in the range 0.5 to 3 μm (Fig. 2(b)). EDS analysis (Fig. 2(c)) reveals the detection of hetero-elements (Si, Al, Mg, Fe, Ca) pertaining to palygorskite in addition to Ti and Cu. This result confirms the coexistence of palygorskite, TiO₂ and CuO particles in mixed CuO-TiO₂/Pal composites.

TEM micrographs show that palygorskite fibers appear bare in the pristine palygorskite Na⁺-Pal (Fig. 3(a)). However, in CuO-TiO₂/Pal composite, the fibers are wrapped and embedded with nodular NPs exhibiting average size

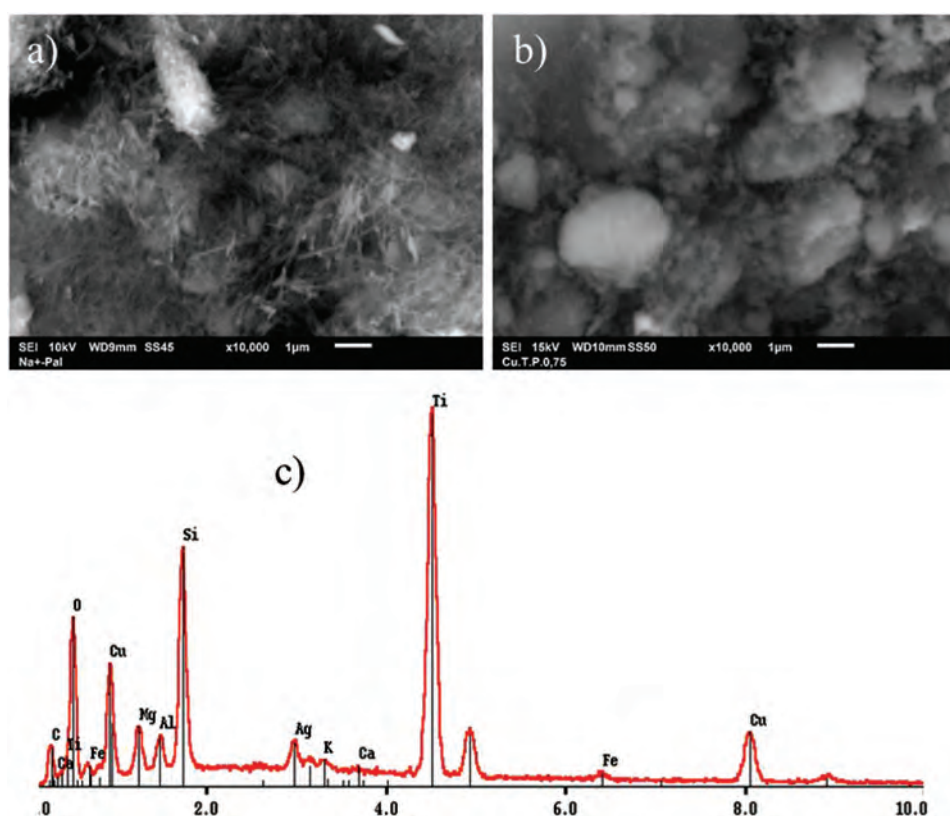


Fig. 2. SEM micrographs of (a) Palygorskite (Na⁺-Pal), (b) 30% CuO-TiO₂/Pal nanocomposite and (c) EDS spectrum recorded on the 30% CuO-TiO₂/Pal nanocomposite (the Ag peak is due to metallization of the sample).

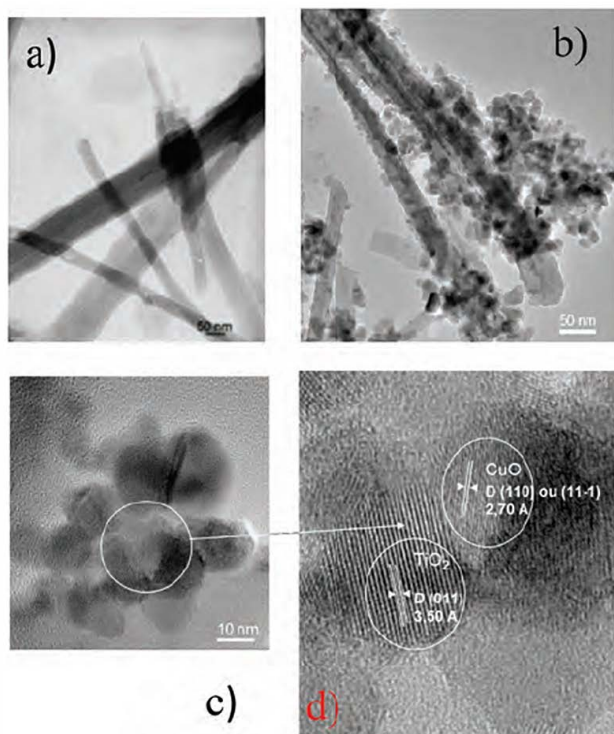


Fig. 3. TEM micrographs of (a) Palygorskite (Na^+ -Pal) and (b) 30% $\text{CuO-TiO}_2/\text{Pal}$ nanocomposite and HRTEM micrographs of 30% $\text{CuO-TiO}_2/\text{Pal}$ nanocomposite showing heterojunctions between the two oxide semiconductors (c and d).

ranging from 6 to 20 nm without distinguishing CuO and TiO_2 (Fig. 3(b)). Oxide NPs have grown directly on the surface of palygorskite fibers to form conformal coatings and by homogeneous nucleation in the free spaces to form aggregates. The presence of these oxide nanoparticles both as aggregates and in the form of conformal coating on palygorskite fibers is likely the main reason to explain the disappearance of palygorskite reflections in XRD patterns of $\text{CuO-TiO}_2/\text{Pal}$ composites (Fig. 1) due to their screening as previously suggested by Bouna et al.¹⁵ Another reason could be the shorter size of the fibers aforementioned (Fig. 2(b)) with a loss of long-range crystallographic order. The nanoparticles forming agglomerates in vicinity of palygorskite fibers appear bigger with a larger size distribution in comparison with those directly supported on fibrous clay mineral. This observation once more confirms the result reported by Bouna et al.¹⁵ in the case of TiO_2 -Pal nanocomposite material regarding the beneficial effect of palygorskite fibers. Heterogeneous nucleation and growth of anatase TiO_2 NPs on the surface of fibers limits significantly their size and prevents their transformation into less photoactive rutile TiO_2 phase.

EDS analysis locally performed on spherical nanoparticles (spectra not reported) confirmed the presence of Ti and Cu. Likewise, selective area electron diffraction (patterns not reported) carried out on spherical NPs show ring patterns which could be indexed on the basis

of anatase TiO_2 or CuO structures. These results further support that nanoparticles supported on palygorskite fibers could be ascribed to anatase TiO_2 along with CuO . Furthermore, High resolution transmission electron microscopy (HRTEM) confirms the quasi spherical shape and the nanometric size of TiO_2 anatase and CuO crystallites as evidenced by Figures 3(c) and (d). In particular, Figure 3(d) shows crystallites of both phases with reticular distances of ca. 0.35 and 0.27 nm corresponding to the $\{101\}$ reflection of anatase and $\{110\}$ or $\{11-1\}$ of CuO respectively. In agglomerates, several particles of the two oxide phases are in contact and consequently they form heterojunctions between the two oxide semiconductors.

3.3. Photocatalytic Activity

The degradation kinetics of OG dye under UV radiation in aqueous solution has been investigated in presence of pristine fibrous clay (Na^+ -Pal), TiO_2/Pal composite and mixed $\text{CuO-TiO}_2/\text{Pal}$ nanocomposites materials differing in the content of CuO (Fig. 4). As expected, the Na^+ -Pal clay mineral does not exhibit any activity to reduce the OG concentration since there is no component in this material known to exhibit photocatalytic properties. Furthermore, the fact that OG concentration is constant during the test means that the adsorption of this model pollutant is negligible on this Na^+ -Pal clay sample in good agreement with Bouna et al.³²

By contrast, the photocatalytic activity of TiO_2/Pal composite is evidenced by the rapid decrease of OG concentration since it is completely degraded after only 150 min. For instance the degradation rate at the origin is approximately 0.010 min^{-1} by considering a first order degradation reaction.

The different $\text{CuO-TiO}_2/\text{Pal}$ mixed nanocomposites exhibit noticeable photocatalytic activity as evidenced by the reduction of OG concentration as the UV irradiation

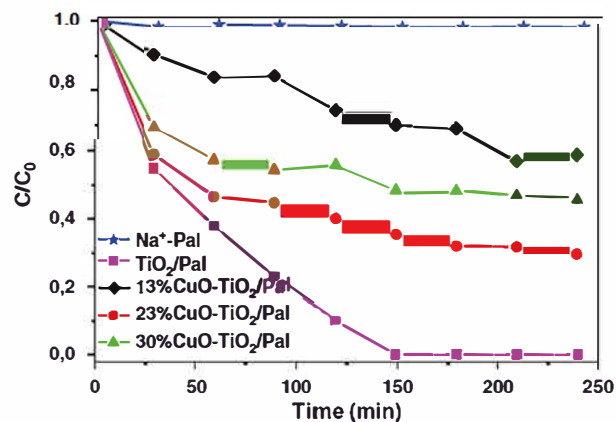


Fig. 4. Change in OG concentration (where C_0 and C are the OG concentrations, respectively, at the initial time $t = 0$, and after an elapsed time t of the photocatalytic reaction) versus UV irradiation time of Na^+ -Pal, TiO_2/Pal composite and $\text{CuO-TiO}_2/\text{Pal}$ mixed nanocomposites differing in CuO content.

time increases. The first characteristic of their photocatalytic behavior is that they are less active than TiO₂/Pal composite. The second is that the degradation curves of OG tend towards a plateau and do not reach 100% degradation even after 4 h of UV irradiation. The 3rd comment about these degradation curves is that there is no clear and simple correlation with a specific characteristic of these mixed nanocomposite photocatalysts such as their composition or microstructure. We grouped in Table I data describing the photocatalytic efficiency as the degradation rate at the origin and the proportion of OG abatement after 120 and 240 min. Also included in this Table I are the mass of each oxide component in the 25 mg of the composite sample used in each photocatalytic test, as well as microstructural features as the average crystallite size determined by XRD.

Figure 4 and data in Table I confirm that the photocatalytic activity of the mixed nanocomposites is not readily correlated with only one of their main features. Although CuO is a semiconductor known to exhibit photocatalytic activity³⁶ it is possible that the quality of CuO NPs formed by our synthesis process are not active because of poor crystallinity or uncontrolled contamination. So assuming that CuO has no intrinsic activity means that the observed global photocatalytic behavior is induced only by the TiO₂ particles and therefore we should see an improvement in activity by increasing the content of TiO₂. Considering that the TiO₂ content changes significantly in the series, it is not what we observe since for instance the richest TiO₂ composite sample is the less active. In fact the TiO₂ content does not change significantly in this series, this assumption does not hold, and this cannot be a key feature to explain the different behaviors, especially because the differences in photocatalytic efficiency are significant.

Among the 3 mixed nanocomposites, the most active is the one that has the mass content of TiO₂ and CuO intermediary. For this composite photocatalyst the degradation rate at the origin (0.009 min⁻¹) is close to that reported for pure CuO (0.016 min⁻¹) for the decomposition of the same pollutant.³⁶ This gives evidences that CuO plays a role in the photocatalytic properties of these composite materials. By increasing the CuO content from 13% to 23% the photocatalytic activity is maximized, e.g., the proportion of OG abatement increases from 28% to 59% after 120 min, while the TiO₂ content is almost the same (13.2 and 12.2 mg) and the average crystallite size of TiO₂ (7.0 ± 0.1 nm) and CuO (10.4 ± 0.3 nm) have not changed (Table I). A further increase in the CuO content from 23% to 30% does not improve the activity but rather it deteriorates since for instance the OG abatement decreases from 59% to 44% after 120 min. In that case, the amount of TiO₂ was almost the same for each test (12.2 and 11.4 mg) and the average crystallite size of CuO was also the same (10.7 nm). The main effect of this further increase of CuO was to deteriorate the crystallinity of TiO₂ NPs since their average crystallite size decreased

from 7.1 to 5.0 nm. When semiconductor crystallites are smaller than a critical value their crystallographic structure is more strongly influenced by the surface structure with an increasing disorder induced by surface reconstruction and defects, which favors recombination of charge carriers and deteriorates the photo-induced properties.

The fact that there is an optimal composition of both TiO₂ and CuO oxides in the mixed supported nanocomposites demonstrates they interact and both oxides contribute to the photocatalysis, probably through heterojunctions, in agreement with TEM observations (Fig. 3). This mechanism generates synergies as this has already been mentioned in the literature.²⁸ Other studies are in progress to confirm the results and to better explain the behavior of these composite photocatalysts.

4. CONCLUSION

Several supported photocatalysts based on CuO–TiO₂/Pal differing in CuO content (13%, 23% and 30%) were synthesized as evidenced by XRD, SEM, TEM and EDS analyses. Spherical nanoparticles of CuO and anatase TiO₂, with crystallite sizes ranging from 6 to 20 nm (TEM and XRD data), were found to be successfully immobilized on palygorskite fibers by forming heterojunctions. The CuO–TiO₂/Pal supported photocatalyst containing 23% of CuO was found to be the most photoactive material towards the degradation of OG dye. Nevertheless, its photoactivity remained lower than that of pure TiO₂ supported on palygorskite from which it originated by impregnation with Cu²⁺ ions.

This preliminary study will be carried on by optimizing synthesis conditions, especially CuO content in CuO–TiO₂/Pal nanocomposites to optimize the crystallite size, their distribution and heterojunctions in order to improve their photocatalytic activity, especially under irradiation in the visible range.

Acknowledgments: The financial supports from the “Convention de coopération CNRST-Maroc/CNRS-France” (chemistry project No. 04/13-14) and the “Programme d’Action Intégrée Toubkal” (No. 14/MS/14-16) are gratefully acknowledged. The authors would like to thank M. C. Lafont for performing TEM analyses.

References and Notes

1. J. Yu, H. Yu, C. H. Ao, S. C. Lee, J. C. Yu, and W. Ho, *Thin Solid Films* 496, 273 (2006).
2. H. Chun, W. Yizhong, and T. Hongxiao, *J. Chemosphere* 41, 1205 (2000).
3. J. Herrmann, *J. Catal. Today* 53, 115 (1999).
4. A. Fujishima, T. N. Rao, and D. A. Tryk, *J. Photochemistry and Photobiology C: Photochemistry Reviews* 1, 1 (2000).
5. S. Chakrabarti and B. K. Dutta, *J. Hazard. Mater.* 112, 269 (2004).
6. D. Robert, A. Piscopo, O. Heintz, and J. V. Weber, *J. Catal. Today* 54, 291 (1999).
7. X. Y. Chuan, M. Hirano, and M. Inagaki, *J. Appl. Catal. B Environ.* 51, 255 (2004).

8. E. P. Reddy, L. Davydov, and P. Smirniotis, *J. Appl. Catal. B Environ.* 42, 1 (2003).
9. S. Nagaoka, Y. Hamasaki, S.-I. Ishihara, M. Nagata, K. Iio, C. Nagasawa, and H. Ihara, *J. Mol. Catal. A Chem.* 177, 255 (2002).
10. P. Aranda, R. Kun, M. A. Martín-Luengo, S. Letáief, I. Dékány, and E. Ruiz-Hitzky, *J. Chem. Mater.* 20, 84 (2008).
11. D. Papoulis, S. Komarneni, D. Panagiotaras, A. Nikolopoulou, H. Li, S. Yin, S. Tsugio, and H. Katsuki, *Appl. Clay Sci.* 83–84, 191 (2013).
12. D. Papoulis, S. Komarneni, D. Panagiotaras, A. Nikolopoulou, K. C. Christoforidis, M. Fernández-García, H. Li, Y. Shu, and T. Sato, *Appl. Clay Sci.* 83–84, 198 (2013).
13. J. Pérez-Carvajal, P. Aranda, S. Obregón, G. Colón, and E. Ruiz-Hitzky, *Microporous Mesoporous Mater.* 222, 120 (2016).
14. G. Zhang, H. Wang, S. Guo, J. Wang, and J. Liu, *Appl. Surf. Sci.* 362, 257 (2016).
15. L. Bouna, B. Rhouta, M. Amjoud, F. Maury, M.-C. Lafont, A. Jada, F. Senocq, and L. Daoudi, *J. Appl. Clay Sci.* 52, 301 (2011).
16. L. Bouna, B. Rhouta, and F. Maury, *International J. Photoenergy* 2013 (2013), ID: 815473.
17. B. Rhouta, L. Bouna, F. Maury, F. Senocq, M. C. Lafont, A. Jada, M. Amjoud, and L. Daoudi, *J. Appl. Clay Sci.* 115, 266 (2015).
18. R. Asahi, T. Morikawa, T. Ohwaki, K. Aoki, and Y. Taga, *Science* 293, 269 (2001).
19. S. Liu, X. Chen, and X. Chen, *J. Chinese J. Catal.* 27, 697 (2006).
20. Q. Wu, W. Li, D. Wang, and S. Liu, *J. Appl. Surf. Sci.* 299, 35 (2014).
21. G. Colón, M. C. Hidalgo, M. Macías, and J. A. Navío, *J. Appl. Catal. A Gen.* 259, 235 (2004).
22. J. Araña, J. M. Doña-Rodríguez, E. TelloRendón, C. Garriga I Cabo, O. González-Díaz, J. A. Herrera-Melián, J. Pérez-Peña, G. Colón, and J. A. Navío, *J. Appl. Catal. B Environ* 44, 161 (2003).
23. J. Araña, J. M. Doña-Rodríguez, E. TelloRendón, C. Garriga I Cabo, O. González-Díaz, J. A. Herrera-Melián, J. Pérez-Peña, G. Colón, and J. A. Navío, *J. Appl. Catal. B Environ.* 44, 153 (2003).
24. T. Umebayashi, T. Yamaki, S. Yamamoto, A. Miyashita, S. Tanaka, T. Sumita, and K. Asai, *J. Appl. Phys.* 93, 5156 (2003).
25. M. Anpo and V. K. Prashant, *Environmentally Benign Photocatalysts*, Berlin (2010).
26. N. Serpone, P. Maruthamuthu, P. Pichat, E. Pelizzetti, and H. Hidaka, *J. Photochem. Photobiol. A Chem.* 85, 247 (1995).
27. L. Zhao, T. Cui, Y. Li, B. Wang, J. Han, L. Han, and Z. Liu, *RSC Adv.* 5, 64495 (2015).
28. M. A. Behnajady and H. Eskandarloo, *J. Chem. Eng.* 228, 1207 (2013).
29. Y. Fang, R. Wang, G. Jiang, H. E. Jin, Y. I. N. Wang, and X. Sun, *J. Bull. Mater. Sci.* 35, 495 (2012).
30. L. Zhang, J. Liu, C. Tang, J. Lv, H. Zhong, Y. Zhao, and X. Wang, *Appl. Clay Sci.* 51, 68 (2011).
31. E. Stathatos, D. Papoulis, C. A. Aggelopoulos, D. Panagiotaras, and A. Nikolopoulou, *J. Hazard. Mater.* 211–212, 68 (2012).
32. L. Bouna, B. Rhouta, M. Amjoud, A. Jada, F. Maury, L. Daoudi, and F. Senocq, *J. Appl. Clay Sci.* 48, 527 (2010).
33. B. Rhouta, E. Zatile, L. Bouna, O. Lakbita, F. Maury, L. Daoudi, M.-C. Lafont, M. Amjoud, F. Senocq, A. Jada, and A. AïtAghzzaf, *J. Physics and Chemistry of Minerals* 40, 411 (2013).
34. J. Araña, C. Fernández Rodríguez, O. González Díaz, J. A. Herrera Melián, and J. P. Peña, *J. Catal. Today* 101, 261 (2005).
35. K. Hofstadler, R. Bauer, S. Novalic, and G. Heisler, *J. Environ. Sci. Technol.* 28, 670 (1994).
36. M. Umadevi and A. Jegatha Christy, *Spectrochimica Acta Part A: Molecular and Biomolecular Spectroscopy* 109, 133 (2013).